Storm in a Teacup: X-Ray View of an Obscured Quasar and Superbubble

George B. Lansbury[1] , Miranda E. Jarvis[2,3], Chris M. Harrison[3] , David M. Alexander[4] , Agnese Del Moro[5],
Alastair C. Edge[4] , James R. Mullaney[6] , and Alasdair P. Thomson[7]

[1] Institute of Astronomy, University of Cambridge, Madingley Road, Cambridge, CB3 0HA, UK; gbl23@ast.cam.ac.uk
[2] Max-Planck Institut für Astrophysik, Karl-Schwarzschild-Str. 1, D-85741 Garching, Germany
[3] European Southern Observatory, Karl-Schwarzschild-Str. 2, D-85748 Garching, Germany
[4] Centre for Extragalactic Astronomy, Department of Physics, Durham University, South Road, Durham, DH1 3LE, UK
[5] Max-Planck-Institut für Extraterrestrische Physik (MPE), Postfach 1312, D-85741, Garching, Germany
[6] Department of Physics and Astronomy, The University of Sheffield, Hounsfield Road, Sheffield, S3 7RH, UK
[7] Jodrell Bank Centre for Astrophysics, School of Physics and Astronomy, The University of Manchester, Alan Turing Building,
Upper Brook Street, Manchester M13 9PL, UK

Abstract

We present the X-ray properties of the "Teacup AGN" (SDSS J1430+1339), a $z = 0.085$ type 2 quasar that is interacting dramatically with its host galaxy. Spectral modeling of the central quasar reveals a powerful, highly obscured active galactic nucleus (AGN) with a column density of $N_H = (4.2\text{–}6.5) \times 10^{23}\,\mathrm{cm}^{-2}$ and an intrinsic luminosity of $L_{2-10\,\mathrm{keV}} = (0.8\text{–}1.4) \times 10^{44}\,\mathrm{erg\,s}^{-1}$. The current high bolometric luminosity inferred ($L_{\mathrm{bol}} \approx 10^{45}\text{–}10^{46}\,\mathrm{erg\,s}^{-1}$) has ramifications for previous interpretations of the Teacup as a fading/dying quasar. High-resolution *Chandra* imaging data reveal a $\approx 10\,\mathrm{kpc}$ loop of X-ray emission, cospatial with the "eastern bubble" previously identified in luminous radio and ionized gas (e.g., [O III] line) emission. The X-ray emission from this structure is in good agreement with a shocked thermal gas, with $T = (4\text{–}8) \times 10^6\,\mathrm{K}$, and there is evidence for an additional hot component with $T \gtrsim 3 \times 10^7\,\mathrm{K}$. Although the Teacup is a radiatively dominated AGN, the estimated ratio between the bubble power and the X-ray luminosity is in remarkable agreement with observations of ellipticals, groups, and clusters of galaxies undergoing AGN feedback.

Key words: galaxies: active – galaxies: evolution – galaxies: individual (Teacup AGN) – quasars: general – X-rays: galaxies

1. Introduction

There is now general agreement that growing supermassive black holes, i.e., active galactic nuclei (AGNs), have a dramatic impact on the evolution of their host galaxies. Observationally constraining the details of this so-called "AGN feedback" is an ongoing challenge of extragalactic astronomy (e.g., Fabian 2012; Heckman & Best 2014; Harrison 2017). There is convincing evidence that powerful radio jets launched by some AGN, whose energetic output is dominated by mechanical energy, are effective at regulating the cold gas supply to their host galaxies (e.g., McNamara & Nulsen 2012). However, it is still unclear how radiatively dominated (or "radio quiet") AGNs interact with their host galaxies (e.g., Mullaney et al. 2013; Greene et al. 2014; Zakamska & Greene 2014), despite these making up the majority of the population (e.g., ∼90% of quasars; Zakamska et al. 2004).

One low-redshift Type 2 quasar ($z = 0.0852$) that has received attention in the literature is SDSS J143029.88 +133912.0. The object has been labeled the "Teacup AGN" due to a "handle" of ionized gas extending ≈10 kpc to the east of the galaxy core, initially identified in SDSS images by Galaxy Zoo (Massimo Mezzoprete, 2007; Lintott et al. 2008) and later confirmed by *HST* imaging (Keel et al. 2012a, 2015). Karl G. Jansky Very Large Array (VLA) data subsequently revealed that radio emission traces this "eastern bubble," and that this is just one of two bipolar radio superbubbles, extending to distances of ≈10 kpc in opposite directions (Harrison et al. 2015). A ≈1 kpc small jet-like feature was also identified, spatially coincident with a ≈700 km s^{-1} outflow of

warm ionized gas, along the same orientation axis as the eastern bubble (Harrison et al. 2015).

On the one hand, the Teacup has been used as a case study for how typical quasars may interact with their host galaxies (Harrison et al. 2014, 2015; Villar Martín et al. 2014; Ramos Almeida et al. 2017). On the other hand, the Teacup has been identified as a "fading"/"dying" quasar, like Hannys Voorwerp (e.g., Keel et al. 2012b; Sartori et al. 2018), where the ionization state of the extended optical emission line region provides evidence that the AGN was more luminous in the past (Gagne et al. 2014; Keel et al. 2017; Villar-Martín et al. 2018). In both cases, it is crucial to have an excellent constraint on the current bolometric luminosity of the central engine—in order to assess (a) the available energy for feedback and (b) the magnitude of AGN fading over time. Furthermore, understanding the physical processes in the bubble is essential for testing both the feedback and fading scenarios. Toward addressing these issues, here we present X-ray constraints on both the central source and the extended bubble of the Teacup. We use $(\Omega_M, \Omega_\Lambda, h) = (0.27, 0.73, 0.70)$.

2. Observations

The X-ray observations of the Teacup are summarized in Table 1. The first X-ray detection of the Teacup was obtained with the XRT instrument on the *Neil Gehrels Swift* observatory, in directors' discretionary time observations (PI: Del Moro). Only ≈19 photons were detected, but the data, nevertheless, hinted at a highly obscured central quasar. A deeper follow-up observation was then performed with *Chandra* (48.4 ks; PI: Harrison), using the Advanced CCD Imaging Spectrometer (ACIS). We process

Table 1
X-Ray Data for the Teacup

Observatory (1)	Obs ID (2)	UT Date (3)	t (4)	S_{net} (5)	B (6)
Chandra ACIS	18149	2016 Apr 19	48.4	702	0
XMM PN	0762630101	2016 May 10	26.7	1625	157
XMM MOS	⋯	⋯	55.8	1862	125
Swift XRT	00033655	2015 Mar	5.5	19	1

Note. (1): Observatory and instrument. (2) and (3): Observation ID and start date, respectively. (4): Net exposure time (ks). (5): Total net source counts in the full-band (i.e., 0.5–8, 0.5–10, and 0.6–10 keV for *Chandra*, *XMM-Newton*, and *Swift* XRT). (6): Background counts in the source region.

the data using the CIAO tool `chandra_repro`.[8] Because there are no periods of significant background flaring, we use the full exposure. The *Chandra* data is the main constituent of this work, used to analyze both the spatially resolved X-ray emission and the central quasar. For the spectral analysis of the quasar, we additionally use data from an *XMM-Newton* observation of the Teacup (PI: Maksym), processed using the *XMM-Newton* Science Analysis Software (SAS v.15.0.0).

3. Results

3.1. X-Ray Imaging

Here we use the *Chandra* imaging (Figure 1) to identify spatially distinct components of the X-ray emission.

The brightest component is the central quasar, which lies at a position of 14:30:29.897+13:39:11.88 in the *Chandra* full-band image. Close to the quasar, we find evidence, from ray-tracing PSF simulations (with `MARX`; Davis et al. 2012), for spatially extended $E \lesssim 1.5$ keV emission on scales of $\approx 0\rlap{.}''6$–$2\rlap{.}''5$ (1–4 kpc). This central extended emission is not a main focus of this paper, but it motivates the relatively small source extraction region adopted in Section 3.2.1.

To the east of the central quasar, there is a striking loop of low-energy (≈ 0.5–1.5 keV) emission extending out to a maximum distance of $\approx 7\rlap{.}''5$ (12 kpc). This X-ray emission traces the morphology of luminous radio emission and ionized gas (e.g., [O III]) in the "eastern bubble" of the Teacup. At higher energies, the bubble is faint but still significant; the photon counts at 1.5–8 and 2–8 keV suggest binomial false probabilities (e.g., Weisskopf et al. 2007) of $P_{false} = 8 \times 10^{-5}$ and 0.005, respectively. We also note that there is tentatively some extended high-energy (1.5–8 keV) emission around the *western* radio bubble, but this has a low significance ($P_{false} = 0.1$).

3.2. X-Ray Spectral Properties

3.2.1. The Central Quasar

For the quasar, we extract source spectra from the *Chandra* and *XMM-Newton* (PN and MOS) data sets, using circular regions of $1''$ and $15''$ radii, respectively. For *XMM-Newton*, we limit the analysis to $E > 2$ keV, where the central point source dominates, based on the high-resolution *Chandra* data. The background spectra are extracted from large source-free regions on the same detector chip as the source. The background-subtracted source spectra are shown in Figure 2.

At 2–8 keV, the *Chandra* flux is a factor of $1.31^{+0.11}_{-0.14}$ higher than *XMM*, in agreement with typical AGN X-ray variability on multi-month timescales (e.g., Yang et al. 2016; Lansbury et al. 2017; Ricci et al. 2017). We model the spectra simultaneously using XSPEC (version 12.9.1p; Arnaud 1996), adopting χ^2 statistics for fitting, and grouping by a minimum of 10 and 20 counts per spectral bin for *Chandra* and *XMM-Newton*, respectively.

The X-ray spectrum rises to higher energies with an observed photon index of $\Gamma_{3-8\,keV} \approx -0.74$, suggesting obscuration by a high column density (N_H) of gas. We thus fit the spectrum with an absorbed power-law model (`cabs · zwabs · pow` in XSPEC formalism). For the intrinsic power law (`pow`), we fix the photon index to a representative value of $\Gamma = 1.9$ and we allow different normalizations for *Chandra* and *XMM-Newton*, given the factor of 1.31 mentioned above. Two additional model components are required: an unobscured power law to parameterize the low-energy ($\lesssim 2$ keV) emission, consistent with electron-scattering of the primary AGN power law; and a narrow redshifted Gaussian to fit Fe Kα line emission at rest-frame $E = 6.4$ keV. This line component is required at the 4.1σ significance level, based on 50,000 simulations of the continuum-only spectrum (using `simftest` in XSPEC). We find no statistical requirement for adding ionized Fe Kα line components to the model (e.g., at 6.7 keV).

The best fit has $\chi^2/n = 1.18$, and the column density is well constrained as $N_H = (4.5 \pm 0.3) \times 10^{23}$ cm^{-2}. The Fe Kα equivalent width of $EW_{FeK\alpha} = 0.12 \pm 0.03$ keV, measured over the absorbed power-law continuum at $E > 4$ keV, is consistent with expectations from the sub-Compton-thick column density. Correcting for absorption, the AGN is intrinsically luminous, with a rest-frame 2–10 keV luminosity of $L_{2-10} = (0.8$–$1.0) \times 10^{44}$ erg s^{-1}.

The above N_H is sufficiently high that Compton-scattered (i.e., "reflected") continuum emission may contribute to the X-ray spectrum. We therefore additionally fit a physically motivated torus model (`borus02`; Baloković et al. 2018), to self-consistently model primary and reflected emission. A statistically acceptable fit is obtained in a basic model setup where the line-of-sight column density (N_H) is untied from the average toroidal column density ($N_{H,tor}$), as expected for a non-uniform torus, and standard values are assumed for the iron abundance (set to solar), the torus covering factor (fixed at 0.5), and the inclination angle (fixed at $87°$). The best fit has $\chi^2/n = 1.12$, $N_H = (5.9^{+0.6}_{-0.5}) \times 10^{23}$ cm^{-2}, $N_{H,tor} = (1.1^{+0.2}_{-0.3}) \times 10^{23}$ cm^{-2}, and $L_{2-10} = (1.1$–$1.4) \times 10^{44}$ erg s^{-1}.

Adding further confidence to these N_H and L_{2-10} values, the Teacup is detected in the *Swift*-BAT 105 month survey (Oh et al. 2018) and the BAT spectrum and luminosity ($L_{14-195} = 1.8 \times 10^{44}$ erg s^{-1}) are consistent with the above best-fit models (Figure 2). The agreement with the BAT spectrum (obtained over ≈ 9 years, up to 2013) suggests that there has been no overall trend of brightening or fading during the full ≈ 11 year period of X-ray coverage, and that the Teacup has maintained a relatively constant average luminosity (within a factor of $\lesssim 2$).

3.2.2. The Eastern Bubble

For the eastern bubble, we extract a *Chandra* spectrum from the region shown in Figure 1, an annular sector at $4\rlap{.}''7$–$9''$ from the central quasar. The region has minimal
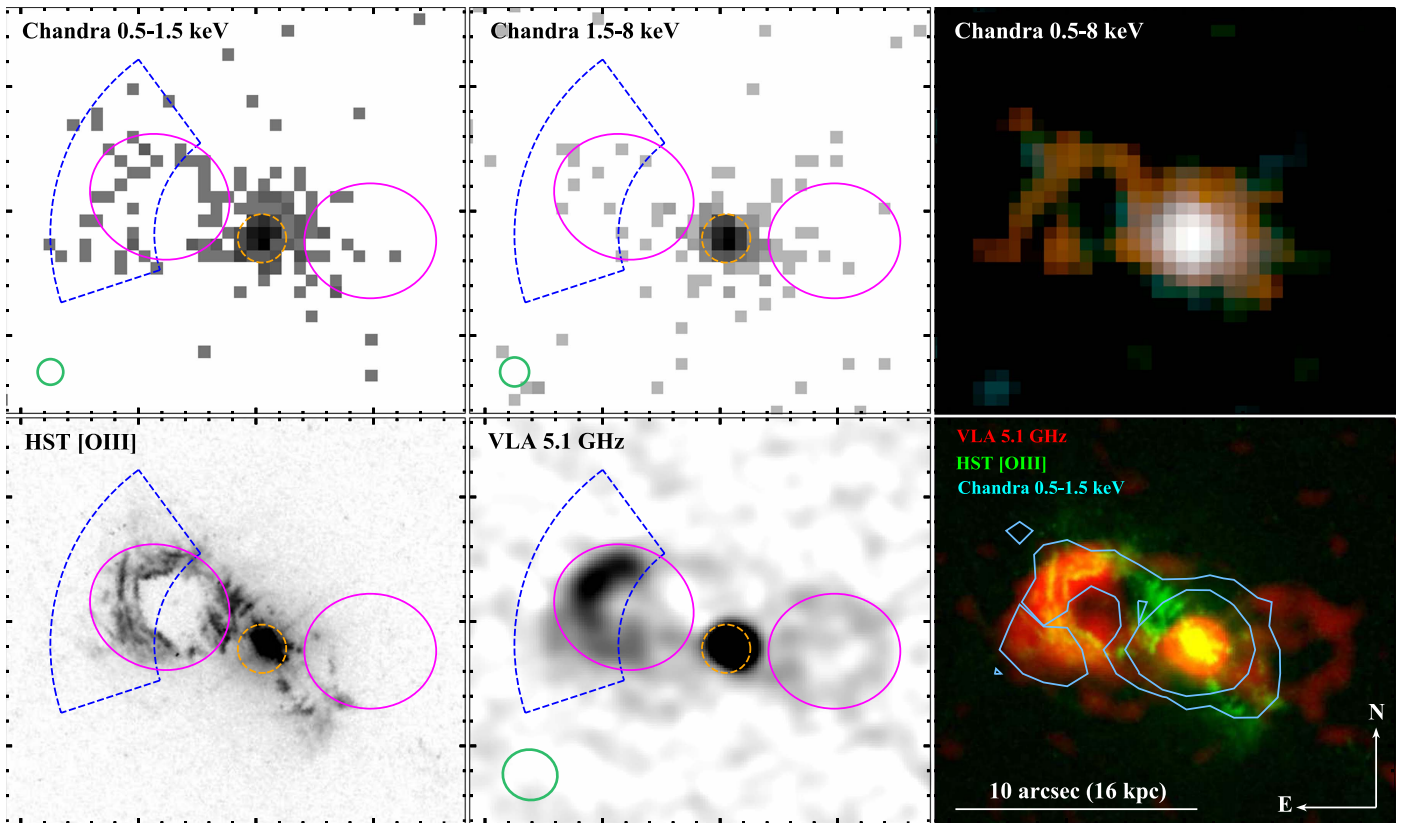
Figure 1. Images of the Teacup from *Chandra* (top row), the [O III] narrowband with *HST* (lower left; Keel et al. 2015), and the VLA at 5.12 GHz (lower middle; Harrison et al. 2015). Magenta elliptical regions highlight the bipolar radio bubble structures. The spectral extraction regions (Section 3.2) are shown in orange and blue. Green ellipses show PSF half-energy widths. Upper right: *Chandra* color composite (smoothed with a 1″ Gaussian) where red, green, and blue correspond to 0.5–1.5, 0.5–8, and 1.5–8 keV, respectively. Lower right: color composite of the radio (red) and [O III] (green) images, with cyan contours showing the spatial distribution of 0.5–1.5 keV emission.

contamination from the quasar PSF (≈ 0.5 photons, based on MARX simulations). The photon counts are low, with 37.5 net source counts (2.5 background counts) at 0.5–8 keV. We therefore adopt the C statistic for fitting,[9] and group the spectrum by a minimum of 1 count per bin.

The bubble spectrum is very steep ($\Gamma_{0.5-8} = 4.9^{+1.1}_{-1.0}$; Figure 3) and comparatively luminous at low energies, with $L_{0.5-2} = (1.3^{+0.3}_{-0.5}) \times 10^{41}$ erg s^{-1}, in agreement with thermal gas emission. We therefore apply the apec model for a collisionally ionized diffuse gas (Smith et al. 2001), which yields a statistically acceptable fit to the data ($C/n = 32/31$; Figure 3), and a normalization of $\eta = 3.9 \times 10^{-6}$. The gas temperature is constrained to be $kT = 0.4^{+0.3}_{-0.1}$ keV, or $T = (3.5-8.1) \times 10^6$ K. This simple single-phase model leaves some positive flux residuals at $\gtrsim 2$ keV, where the X-ray emission is only weakly detected ($\approx 99.5\%$ confidence level; Section 3.1). This excess could plausibly represent an additional hotter gas phase, with $L_{2-10} \approx 1.5 \times 10^{40}$ erg s^{-1} and $kT \gtrsim 2.7$ keV (i.e., $T \gtrsim 3 \times 10^7$ K). The excess is unlikely due to star formation, as the luminosity expectation for such a small volume of the galaxy is significantly lower than 10^{40} erg s^{-1} (e.g., Aird et al. 2017).

We also consider the possibility of a photoionized, rather than thermal, emitter. Based on fits with the photemis model (Kallman & Bautista 2001; which uses XSTAR[10] tables), a

photoionized gas is consistent with the bubble spectrum for an ionization parameter of $\log \xi = 1.7^{+0.3}_{-0.4}$ ($C/n = 32/31$).

4. Discussion

4.1. A Highly Obscured, Luminous Quasar

We have shown that the Teacup quasar is currently accreting at a high luminosity, especially once the line-of-sight obscuration ($N_H \approx 5 \times 10^{23}$ cm^{-2}) is corrected for. The measured X-ray luminosity of $L_{2-10} = (0.8-1.4) \times 10^{44}$ erg s^{-1} implies a high bolometric luminosity (L_{bol}), which is crucial to consider when connecting the energetics of the central engine to phenomena observed in the host galaxy.

In particular, the Teacup has previously been interpreted as a fading/dying quasar due to the observed high-ionization emission line regions (e.g., around the eastern bubble). Photoionization modeling of these regions suggests that the central AGN was more luminous in the past. For instance, Gagne et al. (2014) find a highest past luminosity of $L_{bol}^{past} \approx 2 \times 10^{46}$ erg s^{-1}, in agreement with the results of Villar-Martín et al. (2018) for gas at larger distances (>15 kpc). The extent of any fading since then is crucially dependent on knowledge of the current bolometric luminosity. Fading by factors of $\approx 50-600$ have been inferred to have occured over $\approx (0.4-1) \times 10^5$ year timescales (e.g., Gagne et al. 2014; Keel et al. 2017; Villar-Martín et al. 2018), but this was based on an apparently low current luminosity ($L_{bol} \approx 2 \times 10^{44}$ erg s^{-1}).

The X-ray bolometric correction ($\kappa_{bol} = L_{bol}/L_{2-10}$) is likely to lie in the range $10 \lesssim \kappa_{bol} \lesssim 100$, based on typical

---

9 https://heasarc.gsfc.nasa.gov/docs/xanadu/xspec/wstat.ps
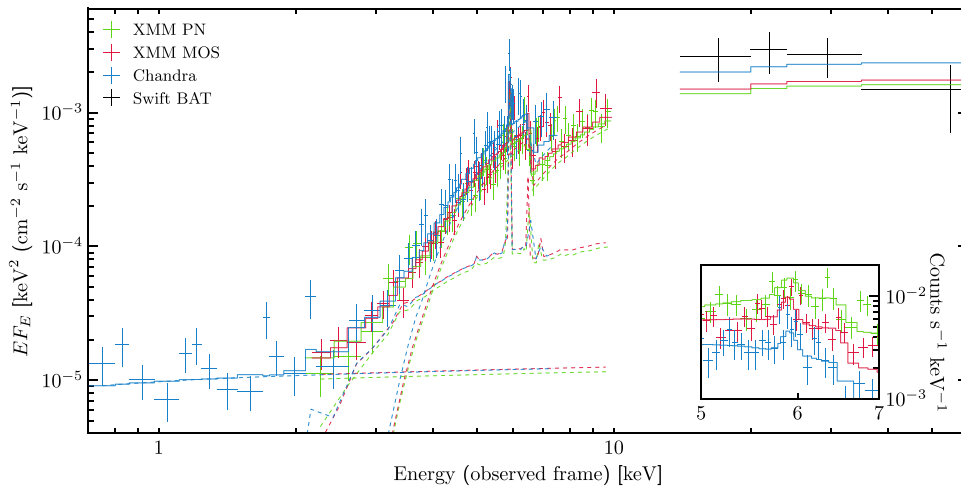10 https://heasarc.gsfc.nasa.gov/docs/software/xstar/xstar.html

Figure 2. X-ray spectra for the central quasar. The solid curves show the `borus02` model best fit to the *Chandra* and *XMM-Newton* spectra, and the dashed lines show the model subcomponents. *Swift*-BAT data, not used in the fitting, are shown for comparison. Inset: zoom-in of the Fe Kα line, in count-rate units.
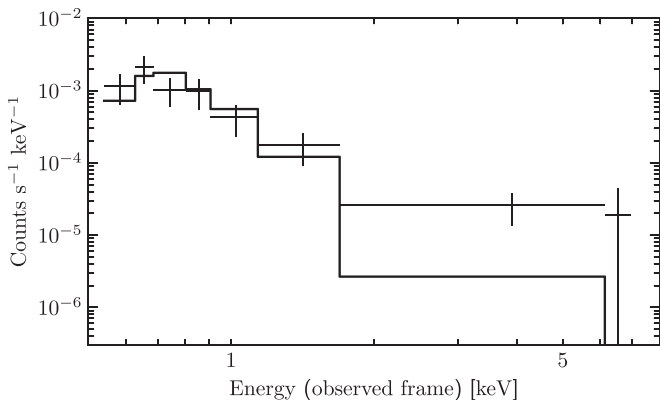

Figure 3. *Chandra* spectrum for the eastern bubble, and the best-fit `apec` model. Each bin has a minimum significance of 2σ, for visual purposes.

values for AGNs (e.g., Vasudevan & Fabian 2009; Vasudevan et al. 2009; Lusso et al. 2012). We therefore find, based on our L_{2-10} constraints, that $8 \times 10^{44} \lesssim L_{bol} \lesssim 1.4 \times 10^{46}\,\mathrm{erg\,s^{-1}}$. This agrees with the luminosity inferred from mid-far-IR SED fitting, $L_{bol} \approx 2 \times 10^{45}\,\mathrm{erg\,s^{-1}}$ (Harrison et al. 2014). Based on the possible L_{bol} values, there is no strong requirement for the Teacup to have undergone a dramatic fading over $\approx 100,000$ years. Assuming an upper limit to the past luminosity of $L_{bol}^{past} \lesssim 2 \times 10^{46}\,\mathrm{erg\,s^{-1}}$, the required fading factor is $\lesssim 25$.

4.2. Understanding the Superbubble

The eastern bubble is luminous in radio emission and spatially coincident high-ionization optical-line emission. Here we have shown that luminous X-ray emission traces the same structure. Below we discuss possible emission mechanisms to explain the X-ray properties.

4.2.1. Photoionized Gas

As shown in Section 3.2.2, a photoionized gas model can describe the bubble X-ray spectrum, for an ionization parameter of $\xi \approx 50\,\mathrm{erg\,cm\,s^{-1}}$. The large distance $(R \approx 10\,\mathrm{kpc})$ is problematic in terms of ionization by the central quasar, however, as the gas density must be low, with $n = L_X / \xi R^2 \approx 0.002\,\mathrm{cm^{-3}}$

(e.g., Kallman & McCray 1982). The implied volume of the gas, estimated from the `photemis` emission measure $(\mathrm{EM} = \int n_e n_H dV)$, is then $\gtrsim$ three orders of magnitude too large compared to the observed volume of the bubble shell. If we assume the quasar had a higher past L_X of $10^{45}\,\mathrm{erg\,s^{-1}}$ (i.e., the same as PDS 456, the most luminous AGN at $z < 0.3$), the required volume is still more than an order of magnitude too high. We therefore prefer the solution presented in Section 4.2.2.

4.2.2. Thermal Gas Resulting from an AGN Outflow

The Teacup radio bubbles were likely formed by jets or quasar winds from the central AGN (e.g., Harrison et al. 2015), which we have confirmed to be intrinsically energetic (Section 4.1). The coupling of such outflows with the interstellar medium can explain the eastern bubble X-ray spectrum, which is consistent with a collisionally dominated thermal gas with $T = (3-8) \times 10^6\,\mathrm{K}$ (Section 3.2.2). In the nearby universe, there are lower luminosity Seyferts with AGN-driven radio bubbles/lobes, where X-ray-emitting gas is found with similar temperatures (e.g., Croston et al. 2008; Mingo et al. 2011, 2012; Paggi et al. 2012). In these cases, the gas is thought to be shock-heated by AGN-driven outflows. The Teacup also bears resemblance to the mechanically driven bubbles/cavities observed at the centers of galaxy groups and clusters (e.g., Bîrzan et al. 2004; Russell et al. 2013). These systems can be morphologically similar to the Teacup in the radio (e.g., Simionescu et al. 2018) and X-ray (e.g., Fabian et al. 2006) bands individually, and there are also a few examples where bright optical line-emitting gas encases the bubble (e.g., Canning et al. 2013). It is not common, however, to observe such a tight spatial correlation between the bright radio and X-ray emission (Figure 1).

We also find a hard X-ray excess in the bubble (Section 3.2.2), which may represent a fainter, hotter X-ray-emitting gas phase, with $T \gtrsim 3 \times 10^7\,\mathrm{K}$. This agrees with expectations for a tenuous but energetic quasar wind (e.g., Strickland & Stevens 2000; Greene et al. 2014; Nims et al. 2015; Costa et al. 2018) that itself shocks cooler gas clouds (e.g., at the edge of the expanding bubble). The latter then emit strongly in low-energy $(T \approx \text{few} \times 10^6\,\mathrm{K})$ X-rays and optical-line emission (e.g., Strickland & Stevens 2000). However, deeper X-ray observations are required to confirm the nature and spatial distribution of this hard X-ray excess.
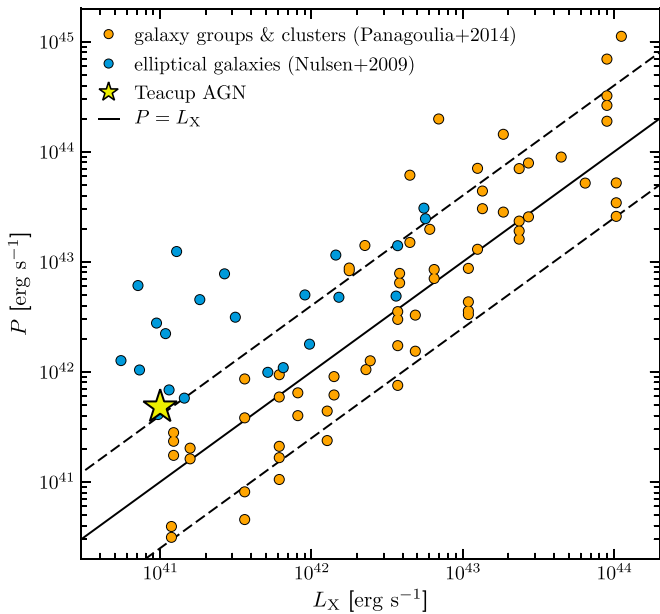
Figure 4. Bubble/cavity power against cooling X-ray luminosity. The Teacup bubble (yellow star) is compared with those in ellipticals (Nulsen et al. 2009), galaxy groups, and clusters (Panagoulia et al. 2014).

Here we consider the physical properties implied for the eastern bubble. Motivated by the X-ray, optical, and radio images, we assume that the gas occupies a 1.7 kpc thick spherical shell. The volume within the bubble extraction region (Figure 1) is then $V = 3 \times 10^{66}$ cm^3. Given the `apec` normalization (η),[11] this implies an electron density of $n_{\rm e} \approx 0.056$ cm^{-3}, and a gas mass of $M \approx 1.6 \times 10^8 \, M_\odot$. Taking the temperature of $kT = 0.4$ keV, and a particle number density of $n = 1.92 n_{\rm e}$, the total thermal energy of the gas is large with $U = (3/2) nkTV \approx 3.1 \times 10^{56}$ erg. Assuming that the energy injection from the central quasar has an age of $t = 20$ Myr, based on the expected local sound speed,[12] the power of the bubble is $P \approx 4.9 \times 10^{41}$ erg s^{-1}. Figure 4 compares this inferred power to the X-ray luminosity of the bubble ($L_{\rm X} \approx 10^{41}$ erg s^{-1}; Section 3.2.2). As shown, the ratio $P/L_{\rm X}$ is in agreement with the relationship between heating power and cooling X-ray luminosity found for bubbles/cavities in ellipticals, groups, and clusters undergoing mechanically dominated AGN feedback (e.g., Fabian 2012, McNamara & Nulsen 2012, Panagoulia et al. 2014). Although these bubbles do not typically resemble the Teacup morphology across all wavelengths, Figure 4 provides some evidence for similarities between the physical mechanisms of AGN feedback in these systems.

5. Summary

In this work, we have characterized the Teacup AGN and host galaxy, in terms of their X-ray properties. The main results are as follows:

1. The high-resolution *Chandra* images reveal a striking loop of X-ray emission, extending to $\approx$10 kpc. This is spatially coincident with the well-known eastern bubble, luminous in radio emission and ionized gas.

2. Modeling the *Chandra* and *XMM-Newton* spectra of the central quasar, we find it to be highly obscured, with $N_{\rm H} = (4.2\text{–}6.5) \times 10^{23}$ cm^{-2}, and intrinsically luminous, with $L_{2\text{–}10\,{\rm keV}} = (0.8\text{–}1.4) \times 10^{44}$ erg s^{-1}. The quasar is inferred to be currently accreting at a high bolometric luminosity ($L_{\rm bol} \approx 10^{45}\text{–}10^{46}$ erg s^{-1}). We therefore find no strong requirement for a fading/dying quasar scenario to explain the ionized gas emission in the eastern bubble.

3. X-ray emission from the eastern bubble is spectrally consistent with a thermal (e.g., shock-heated) gas of temperature $kT = 0.4^{+0.3}_{-0.1}$ keV. There is also evidence for a fainter component of $kT \gtrsim 2.7$ keV gas, in agreement with a quasar wind, but deeper observations are required to study this hotter gas phase.

4. The ratio between the inferred bubble power ($P \approx 4.9 \times 10^{41}$ erg s^{-1}) and the X-ray luminosity ($L_{\rm X} \approx 10^{41}$ erg s^{-1}) is remarkably similar to that seen for bubbles/cavities in ellipticals, galaxy groups, and clusters undergoing mechanically dominated AGN feedback. Our observations of the Teacup provide evidence of similar feedback processes at work in a quasar.

ORCID iDs

George B. Lansbury ⓘ https://orcid.org/0000-0002-5328-9827
Chris M. Harrison ⓘ https://orcid.org/0000-0001-8618-4223
David M. Alexander ⓘ https://orcid.org/0000-0002-5896-6313
Alastair C. Edge ⓘ https://orcid.org/0000-0002-3398-6916
James R. Mullaney ⓘ https://orcid.org/0000-0002-3126-6712

References

Aird, J., Coil, A. L., & Georgakakis, A. 2017, MNRAS, 465, 3390
Arnaud, K. A. 1996, in ASP Conf. Ser. 101, Astronomical Data Analysis Software and Systems V, ed. G. H. Jacoby & J. Barnes (San Francisco, CA: ASP), 17
Baloković, M., Brightman, M., Harrison, F. A., et al. 2018, ApJ, 854, 42
Bîrzan, L., Rafferty, D. A., McNamara, B. R., Wise, M. W., & Nulsen, P. E. J. 2004, ApJ, 607, 800
Canning, R. E. A., Sun, M., Sanders, J. S., et al. 2013, MNRAS, 435, 1108
Costa, T., Rosdahl, J., Sijacki, D., & Haehnelt, M. G. 2018, MNRAS, 473, 4197
Croston, J. H., Hardcastle, M. J., Kharb, P., Kraft, R. P., & Hota, A. 2008, ApJ, 688, 190
Davis, J. E., Bautz, M. W., Dewey, D., et al. 2012, Proc. SPIE, 8443, 84431A
Fabian, A. C. 2012, ARA&A, 50, 455
Fabian, A. C., Sanders, J. S., Taylor, G. B., et al. 2006, MNRAS, 366, 417
Gagne, J. P., Crenshaw, D. M., Kraemer, S. B., et al. 2014, ApJ, 792, 72
Greene, J. E., Pooley, D., Zakamska, N. L., Comerford, J. M., & Sun, A.-L. 2014, ApJ, 788, 54
Harrison, C. M. 2017, NatAs, 1, 0165
Harrison, C. M., Alexander, D. M., Mullaney, J. R., & Swinbank, A. M. 2014, MNRAS, 441, 3306
Harrison, C. M., Thomson, A. P., Alexander, D. M., et al. 2015, ApJ, 800, 45
Heckman, T. M., & Best, P. N. 2014, ARA&A, 52, 589

---

[11] $\eta = 10^{-14}(4\pi)^{-1}[D_{\rm A}(1+z)]^{-2} \int n_{\rm e} n_{\rm H} dV$, where $D_{\rm A}$ is the angular diameter distance.
[12] The local speed of sound is determined as $c_{\rm s} = \sqrt{\gamma kT / \mu m_{\rm H}}$, where $\gamma = 5/3$, $\mu = 0.61$, and $m_{\rm H}$ is the atomic mass of hydrogen.

Kallman, T., & Bautista, M. 2001, ApJS, 133, 221
Kallman, T. R., & McCray, R. 1982, ApJS, 50, 263
Keel, W. C., Chojnowski, S. D., Bennert, V. N., et al. 2012a, MNRAS, 420, 878
Keel, W. C., Lintott, C. J., Maksym, W. P., et al. 2017, ApJ, 835, 256
Keel, W. C., Lintott, C. J., Schawinski, K., et al. 2012b, AJ, 144, 66
Keel, W. C., Maksym, W. P., Bennert, V. N., et al. 2015, AJ, 149, 155
Lansbury, G. B., Stern, D., Aird, J., et al. 2017, ApJ, 836, 99
Lintott, C. J., Schawinski, K., Slosar, A., et al. 2008, MNRAS, 389, 1179
Lusso, E., Comastri, A., Simmons, B. D., et al. 2012, MNRAS, 425, 623
McNamara, B. R., & Nulsen, P. E. J. 2012, NJPh, 14, 055023
Mingo, B., Hardcastle, M. J., Croston, J. H., et al. 2011, ApJ, 731, 21
Mingo, B., Hardcastle, M. J., Croston, J. H., et al. 2012, ApJ, 758, 95
Mullaney, J. R., Alexander, D. M., Fine, S., et al. 2013, MNRAS, 433, 622
Nims, J., Quataert, E., & Faucher-Giguère, C.-A. 2015, MNRAS, 447, 3612
Nulsen, P., Jones, C., Forman, W., et al. 2009, in AIP Conf. Ser. 1201, The Monster's Fiery Breath: Feedback in Galaxies, Groups, and Clusters, ed. S. Heinz & E. Wilcots (Melville, NY: AIP), 198
Oh, K., Koss, M., Markwardt, C. B., et al. 2018, ApJS, 235, 4
Paggi, A., Wang, J., Fabbiano, G., Elvis, M., & Karovska, M. 2012, ApJ, 756, 39
Panagoulia, E. K., Fabian, A. C., Sanders, J. S., & Hlavacek-Larrondo, J. 2014, MNRAS, 444, 1236

Ramos Almeida, C., Piqueras López, J., Villar-Martín, M., & Bessiere, P. S. 2017, MNRAS, 470, 964
Ricci, C., Trakhtenbrot, B., Koss, M. J., et al. 2017, ApJS, 233, 17
Russell, H. R., McNamara, B. R., Edge, A. C., et al. 2013, MNRAS, 432, 530
Sartori, L. F., Schawinski, K., Koss, M. J., et al. 2018, MNRAS, 474, 2444
Simionescu, A., Tremblay, G., Werner, N., et al. 2018, MNRAS, 475, 3004
Smith, R. K., Brickhouse, N. S., Liedahl, D. A., & Raymond, J. C. 2001, ApJL, 556, L91
Strickland, D. K., & Stevens, I. R. 2000, MNRAS, 314, 511
Vasudevan, R. V., & Fabian, A. C. 2009, MNRAS, 392, 1124
Vasudevan, R. V., Mushotzky, R. F., Winter, L. M., & Fabian, A. C. 2009, MNRAS, 399, 1553
Villar-Martín, M., Cabrera-Lavers, A., Humphrey, A., et al. 2018, MNRAS, 474, 2302
Villar Martín, M., Emonts, B., Humphrey, A., Cabrera Lavers, A., & Binette, L. 2014, MNRAS, 440, 3202
Weisskopf, M. C., Wu, K., Trimble, V., et al. 2007, ApJ, 657, 1026
Yang, G., Brandt, W. N., Luo, B., et al. 2016, ApJ, 831, 145
Zakamska, N. L., & Greene, J. E. 2014, MNRAS, 442, 784
Zakamska, N. L., Strauss, M. A., Heckman, T. M., Ivezić, Ž, & Krolik, J. H. 2004, AJ, 128, 1002